Radiation Hardness of Perovskite Solar Cells Based on Aluminum-Doped Zinc Oxide Electrode under Proton irradiation

Jérémy Barbé,[1] Declan Hughes,[1] Zhengfei Wei,[1] Adam Pockett,[1] Harrison K. H. Lee,[1] Keith C. Heasman,[2] Matthew J. Carnie,[1] Trystan M. Watson,[1] and Wing C. Tsoi[1]

[1]SPECIFIC, College of Engineering, Swansea University, Bay Campus, Fabian Way, Swansea, SA1 8EN, UK

E-mail: w.c.tsoi@swansea.ac.uk

[2]Ion Beam Centre, Advanced Technology Institute, University of Surrey, Guildford, Surrey, GU2 7XH, UK

ABSTRACT

Due to their high specific power and potential to save both weight and stow volume, perovskite solar cells have gained increasing interest to be used for space applications. However, before they can be deployed into space, their resistance to ionizing radiations such as high-energy protons must be demonstrated. In this report, we investigate the effect of 150 keV protons on the performance of perovskite solar cells based on aluminium-doped zinc oxide (AZO) transparent conducting oxide (TCO). Record power conversion efficiency of 15% and 13.6% were obtained for cells based on AZO under AM1.5G and AM0 illumination, respectively. We demonstrate that perovskite solar cells can withstand proton irradiation up to 10^{13} protons.cm^{-2} without significant loss in efficiency. At this irradiation dose, Si or GaAs solar cells would be completely or severely degraded when

exposed to 150 keV protons. From 10^{14} protons.cm^{-2}, a decrease in short-circuit current of the perovskite cells is observed, which is consistent with interfacial degradation due to deterioration of the Spiro-OMeTAD HTL during proton irradiation. Using a combination of non-destructive characterization techniques, results suggest that the structural and optical properties of perovskite remain intact up to high fluence levels. Although shallow trap states are induced by proton irradiation in perovskite bulk at low fluence levels, they can release charges efficiently and are not detrimental to the cell's performance. This work highlights the potential of perovskite solar cells based on AZO TCO to be used for space applications and give a deeper understanding of interfacial degradation due to proton irradiation.

KEYWORDS: Perovskite solar cells, proton irradiation, space, aluminium-doped zinc oxide

INTRODUCTION

Perovskite solar cells have recently attracted lots of attention in the scientific community due to their rapid progress in efficiency and potentially low manufacturing costs[1]. Using solution-based processes, perovskite materials can be fully printed at low temperature on light-weight flexible substrates[2][3][4], which has an enormous potential for a wide range of applications. Among them, researchers have only recently considered the use of perovskite for aerospace and space applications. Today, it costs around $20,000 to put a kilogram of payload in earth orbit[5] (destinations beyond geosynchronous orbits require significantly higher launch costs) and solar panels can represent a large fraction of satellites or probes total weight. In 2015, a single-junction perovskite solar cell with super high specific power (power-per-weight) of 23 W.g^{-1} under Air Mass 1.5 Global (AM1.5G) illumination has been demonstrated[6]. In comparison, commercial triple junction solar cells based on GaAs developed by Azur Space® have much lower specific power of 0.5 W.g^{-1} under AM0 (zero air mass) illumination[7]. Besides, flexible solar panels such as roll-out solar arrays (ROSA) deployed in space by NASA in 2017 can be very compact in size and have the potential to save stow volume during launch[5]. Hence, perovskite solar cells have

key advantages to be used in space missions for which payload control is crucial. Besides, perovskite solar cells limitations on earth such as lead toxicity and degradation due to humidity and oxygen molecules are no longer an issue in space.

However, outer space is flooded with radiations such as electrons, protons, neutrons, X-rays or gamma rays which can have dramatic consequences on microelectronic components. These high-energy particles are known to cause damages in semiconductors through ionization and displacement[8]. For example, although GaAs solar cells are the most prominent solar technology used in space due to their high efficiency, they are particularly sensitive to radiation and can undergo more than 80% decrease in output power after irradiation with 150 keV protons at 10^{12} particles.cm^{-2} fluence[9] or with 1 MeV protons at 10^{13} particles.cm^{-2} fluence[10]. The radiation hardness of perovskite solar cells has been little investigated and is the subject of a few publications only[11][12][13][14][15][16][17]. In 2018, Miyasaka *et al.* studied the radiation tolerance of perovskite solar cells composed of a mesoporous TiO_2 electrons transport layer (ETL) and P3HT holes transport layer (HTL) to 1 MeV electrons and 50 keV protons and found that cells can survive to accumulated dose of 10^{16} electrons.cm^{-2} and 10^{15} protons.cm^{-2}, respectively[14]. For this study, P3HT was chosen as a HTL for its better thermal resistance as compared to Spiro-OMeTAD, which is known to degrade at 80-100°C. P3HT showed robust radiation stability but the power conversion efficiency (PCE) was rather low (4 to 5%) compared to state-of-the-art perovskite solar cells with Spiro-OMeTAD HTL (>20%). The radiation hardness of p-i-n $MAPbI_3$ (inverted-type) solar cells to protons irradiation was also investigated by two other groups[13][11][17]. Huang et al. showed that 50 keV protons with fluence 10^{12} cm^{-2} cause significant degradation of the performance of inverted perovskite cells, but these cells can be restored with a vacuum annealing process. Lang et al. showed that the cells exposed to 20 MeV and 68 MeV proton irradiation from the substrate side could withstand protons dose up to 10^{12} protons.cm^{-2} without significant damages. While experiments such as these, with high energy protons, are useful in looking at extreme cases of radiation bombardment and associated degradation, the realistic energy levels of protons in space are, statistically, much lower. Proton's with energy between 50 and 200 keV occur at a flux of ~1E7 higher than protons at >20 MeV and are therefore a more relevant energy range to investigate.

In this work, we present a detailed study on the effect of 150 keV protons on the performance of perovskite solar cells fabricated on quartz substrates coated with aluminium-doped zinc oxide (AZO) transparent conducting oxide (TCO). Owing to the low-cost, nontoxicity and abundance, AZO thin films could be a better alternative to ITO and FTO films[18]. Besides, AZO is radio-frequency (RF) sputtered at room temperature and can be deposited on flexible substrates. Although room-temperature processed AZO is known for its relative poor resistance to moisture[19][20], this issue could be mitigated for use in space where moisture is absent and by encapsulation. Here, record AM1.5G PCE up to 15% was obtained with AZO TCO, SnO_2 ETL, triple cation perovskite and Spiro-OMeTAD HTL. We also report the AM0 efficiency with a champion cell having up to 13.6% PCE. Although Spiro-OMeTAD is not thermally stable, it could be used for space missions to the outer regions of the solar system which wouldn't require solar cells to be exposed to high temperature. Besides, it could be used on earth in regions with radioactive pollution like damaged nuclear power plants, which were proposed to be rehabilitated as solar plants, providing that solar cells have a high radiation hardness[16]. Besides, SnO_2 was used here as an ETL instead of mp-TiO_2. Indeed, mp-TiO_2 is known to be highly sensitive to UV light and acts as a catalyst to the degradation of the perovskite layer. On the contrary, SnO_2 has been shown to have much higher stability against UV irradiation[21], which is particularly important in space as the AM0 spectrum contains a higher level of UV radiation.

These devices were exposed to 150 keV proton irradiation from 10^{12} to 10^{15} protons.cm^{-2}. We demonstrate that the cells can withstand proton irradiation up to 10^{13} protons.cm^{-2} without significant loss in efficiency. The optical and structural properties of individual layers in the device stack were measured by X-ray diffraction (XRD), UV-Vis, Raman and photoluminescence spectroscopy, and the impact of proton irradiation on recombination within the devices was measured by transient photovoltage (TPV). It was shown that the efficiency loss observed starting from 10^{14} protons.cm^{-2} can be ascribed to the degradation of the Spiro-OMeTAD HTL.

RESULTS AND DISCUSSION

Figure 1(a) shows the histogram of perovskite solar cells efficiencies fabricated on quartz/AZO substrates before proton irradiation. Quartz was used instead of soda-lime glass which can be darkened by radiations[15]. Glass darkening is a well-known effect of ionizing radiations and space-

qualified glass made of ultra-thin cerium doped glass is usually used to prevent this effect for satellites and other space applications. Quartz is used here to avoid any parasitic effect due to the substrate and assess the effect of radiations on the layer stack only. As observed in figure 1(a), the performances of the cells under AM1.5G illumination vary between 8% and 15%, mostly due to variations in J_{sc} and FF (not shown). To the best of our knowledge, the champion cell with PCE of 14.95% outperforms previous works on perovskite solar cells fabricated on AZO by almost 3% increase in absolute efficiency[22][23][24][25]. We have also measured the efficiency under AM0 illumination, which reached up to 13.6% PCE with J_{sc} of 26.6 mA.cm^{-2}. The J-V curves under AM1.5G and AM0 illumination for the champion cell are shown in figure 1(b). Due to the rather large range of PCEs obtained, it was decided to select one sample with PCEs < 11% and one sample with PCEs >11% to be exposed to each protons fluence (as well as for the control samples not exposed to proton irradiations).

Then, the samples were irradiated with 150 keV protons with fluence ranging from 10^{12} to 10^{15} protons.cm^{-2}. Some devices were not exposed to proton irradiation but subjected to the same atmospheric conditions to serve as a reference. The value of 150 keV for the energy of protons is commonly used for other types of PV such as Si or GaAs[26][9]. We have performed simulations using the program SRIM/TRIM to assess the effect of 150 keV protons on planar solar cells with AZO/quartz substrates. In figure S1, it can be seen when samples are irradiated from the gold side, collisions take place in all layers from the top contact (gold) to the bottom contact (AZO). This is thus a good energy to probe the radiation hardness of perovskite solar cells. SRIM/TRIM simulation were also performed from the quartz side (figure S2) and indicate that in this case all protons are stopped in the first 230 nm of the quartz, never reaching the perovskite stack. Hence, the cells were implanted from the gold side to directly probe the effect of 150 keV protons on the perovskite stability. In figure S1, it can be seen that many protons collisions take place in the AZO layer. Therefore, the TCO is also critical to the stability of the perovskite solar cells. As shown in figure 1(c), the optical properties of AZO/quartz are unchanged after proton irradiation up to a fluence of 10^{15} protons.cm^{-2}, which is a clear indication that AZO can withstand very high proton irradiation without being damaged. Besides, a significant fraction of protons collide atoms in the perovskite layer near the SnO_2 interface, as well as in the Spiro HTL. This allows to investigate the effect of proton irradiation not only in the TCO, but in the active layer and extraction layers as well.

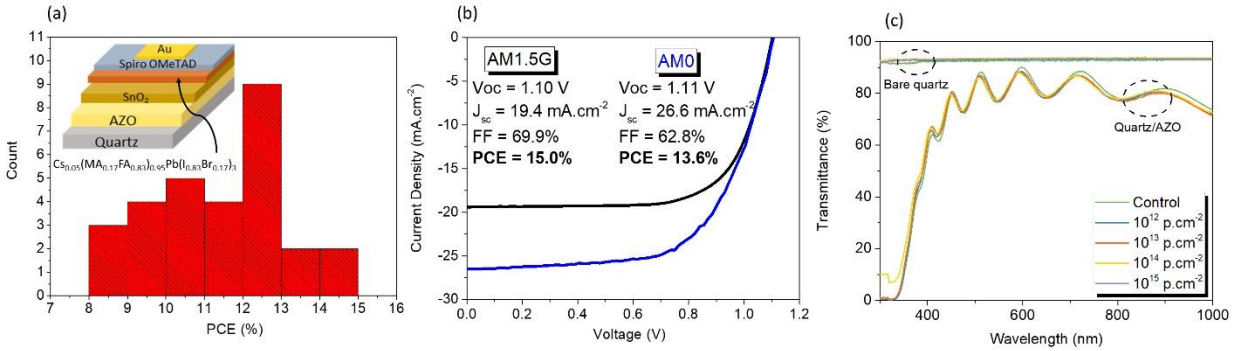

Figure. 1 (a) Histogram of power conversion efficiency (PCE) for perovskite solar cells with structure quartz/AZO/SnO_2/$Cs_{0.05}(MA_{0.17}FA_{0.83})_{0.95}Pb(I_{0.83}Br_{0.17})_3$/Spiro/Au. (b) J-V curves under AM1.5G and AM0 illumination for champion cell. (c) Transmittance spectra of bare quartz and quartz/AZO substrates after protons bombardment with various fluences.

The changes in PV parameters (J_{sc}, FF, V_{oc} and PCE) after proton irradiation are shown in Figure 2(a). The remaining factor was calculated by dividing the PV parameters after proton irradiation by the PV parameters for the same set of cells (ie. for each fluence) before proton irradiation. Interestingly, the PCE slightly improved for the control sample, which travelled to the Ion Beam Center in Surrey with the other samples but was not irradiated. All samples were kept under N_2 in the dark before the irradiation was carried out, and then kept for a week under dark air before they could be measured after irradiation. The PCE is slightly improved at 10^{12} cm^{-2} fluence and slightly decreased at 10^{13} cm^{-2} fluence, as compared to the control sample. At 10^{14} cm^{-2} fluence, a prominent decrease is observed, and the PCE remaining factor is reduced to 0.2, which is due to a decrease in J_{sc} and FF, while the V_{oc} remains almost constant. At 10^{15} cm^{-2} fluence, a very low current was measured as the cells were highly degraded, but the cells still had a non-negligible V_{oc} of 0.8 V. The fact that the V_{oc} remains high until 10^{15} cm^{-2} proton fluence suggests that the perovskite layer itself is not significantly degraded, while the decrease in FF and J_{sc} can be explained by a deterioration of charge extraction properties due to the degradation of spiro-OMeTAD or SnO_2 interlayers[27]. The remaining factors were also measured under AM0 illumination and are shown in figure S3, indicating similar trend as under AM1.5G illumination. The external quantum efficiency (EQE) for representative cells at each protons fluence is shown in Figure 2(b). The results are in good agreement with the J_{sc} trend obtained from current-voltage measurements, showing a stable EQE up to 10^{13} protons.cm^{-2} (interferences are due to the 700 nm-

thick AZO layer) and then significant decrease at 10^{14} protons.cm^{-2}. The decrease in EQE is uniform across the whole spectrum range and affects equally the UV and visible parts. On the contrary, Miyasawa et al. measured a non-uniform spectral response of photocurrent of FAMAPb(IBr)$_3$ cells after proton irradiation at fluence 10^{14} protons.cm^{-1},[14]which was ascribed to degradation of the active layer. Here, the uniform decrease of the EQE spectrum could be indicative of a deterioration of the charge extraction properties rather than charge generation properties and points out the role of charge extraction layers in the degradation of the solar cells during irradiation. At 10^{15} protons.cm^{-2}, the EQE is almost null and barely visible on the figure. Hence, from these measurements it is clear that perovskite solar cells with Spiro OMeTAD HTL can be exposed to a radiation level up to 10^{13} protons.cm^{-2} without being significantly degraded. By comparison, the V_{oc} and J_{sc} of Si solar cells exposed to 150 keV protons decrease by more than 40% and 10%, respectively, at 10^{13} protons.cm^{-2}[26]. Besides, it was demonstrated that GaAs solar cells exposed to 150 keV protons start to degrade at a radiation dose as low as 10^{10} protons.cm^{-2} and the remaining factor for P_{max} is decreased to 0.2 at 10^{12} protons.cm^{-2}[9]. In our case, a P_{max} remaining factor of 0.2 is reached only at 10^{14} protons.cm^{-2}, which means that perovskite solar cells have at least two orders of magnitude higher tolerance to proton irradiation than GaAs solar cells.

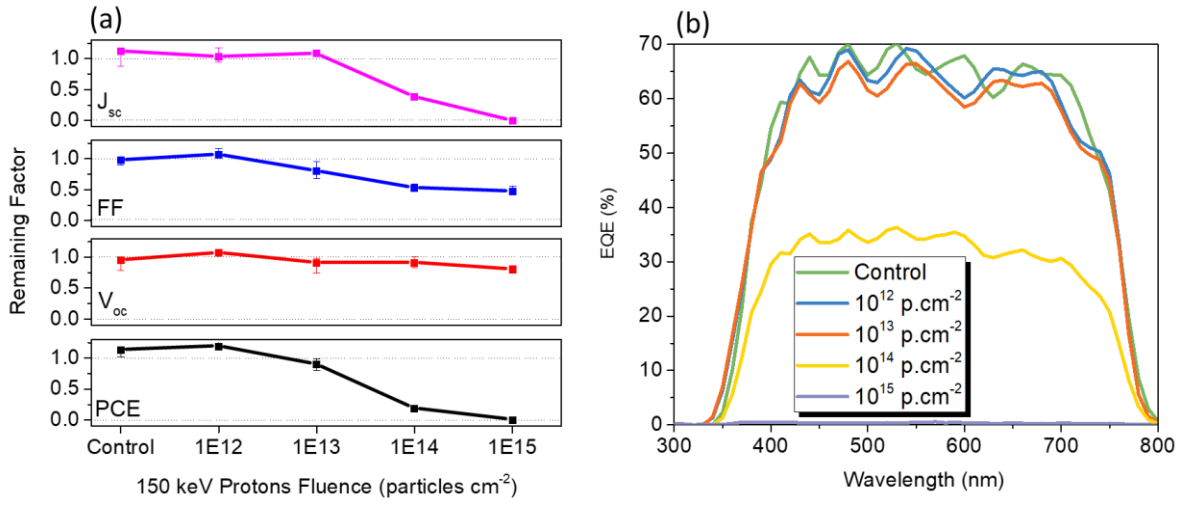

Figure. 2 (a) Changes of photovoltaic characteristics (J_{sc}, FF, V_{oc}, and PCE) of perovskite solar cells under AM1.5G illumination as a function of protons fluence. Averaged values measured for a total of 6 different cells for each fluence. (b) External quantum efficiency for representative devices as a function of protons fluence.

Next, we used a combination of non-destructive techniques to investigate the degradation mechanisms in perovskite solar cells and perovskite films after proton irradiation and have a better understanding of the degradation of individual layers in the device stack.

The X-ray diffraction (XRD) spectra of perovskite films deposited on quartz and exposed to irradiation with 10^{14} and 10^{15} protons.cm^{-2} are shown in figure 3(a) and compared to a non-irradiated control sample. For all samples, a PbI_2 peak can be observed at 12.7°, which is ascribed to the 5% PbI_2 excess used in the precursor solution and/or to environmental degradation (samples were measured more than 40 days after fabrication). However, all samples have similar spectra. The normalized spectra (figure S4) show perfect overlap of the (110) perovskite peak for the three samples and similar intensity ratio between PbI_2 and perovskite peaks. This indicates no degradation of the crystalline structure of the triple cation perovskite film due to protons irradiation.

Reflectance spectra of perovskite films on quartz with gold electrode are shown in figure 3(b). Any changes in perovskite absorbance would appear on the reflectance spectra (measured from quartz side). The perovskite band edge is clearly visible at 740-775 nm for all three samples and all spectra in the range 200-775 nm are very similar (intensity differences above 775 nm is not related to perovskite and can be ascribed to gold thickness variations). We note however that the sample irradiated with 10^{15} protons.cm^{-2} has a slightly different spectral shape in the range 650-700 nm and 200-300 nm. This could suggest that perovskite has undergone some degradation for the highest proton fluence, although it may not fully explain the strong PCE drop measured for this sample.

The photoluminescence (PL) intensity of the full device stack after proton irradiation is shown in Figure 3(a). The PL intensity undergoes almost three folds increase in magnitude after irradiation with 10^{12} protons.cm^{-2} as compared to the reference sample. This can be correlated with the slight increase in PCE after irradiation with 10^{12} protons.cm^{-2} and suggests that the performance of perovskite solar cells could be improved after 150 keV proton irradiation with mild fluence. However, from 10^{13} protons.cm^{-2} onwards, we observe a constant decrease of the PL intensity, in good agreement with the decrease in PV performance. The PL intensity is indicative of the quality of the perovskite bulk or interfaces. Deep trap states formed in the perovskite bulk can induce non-radiative recombination and quench the PL[28][29]. However, in a full device stack, a defective interface due to degradation of the electrons or holes extraction layers can also quench the PL if

carriers are lost to nonradiative recombination in the contact and no longer return to the perovskite[30]. Hence, these results show that the PL intensity follows the same trend as the power conversion efficiency after proton irradiation, but at this stage it cannot be clearly attributed to specific damage in the perovskite bulk or in the electron/hole transport layers.

The Raman spectra of Spiro-OMeTAD after irradiation are shown in figure 3(b). The results were averaged over 100 spectra measured for each sample to account for local non-uniformities. Besides, at least two samples were measured for each fluence to confirm the results. The integrity of Spiro-OMeTAD is clearly maintained up to 10^{13} protons.cm^{-2} as the spectra remain unchanged, showing sharp and intense signal from Spiro-OMeTAD[32]. However, some degradation is observed at 10^{14} protons.cm^{-2} where the peaks intensity starts to decrease, and even stronger degradation of the spiro-OMeTAD is observed at 10^{15} protons.cm^{-2}. As the Raman intensity can be sensitive to measurement conditions (especially to the focus), normalized spectra are also shown in figure S5 in SI. After normalization, all spectra up to 10^{13} protons.cm^{-2} overlap each other perfectly, indicating no change in spiro-OMeTAD chemical structure. However, at 10^{14} and 10^{15} protons.cm^{-2}, it is clear that some modes are attenuated such as 755 cm^{-1} or 914 cm^{-1} peaks, and the shape of the spectrum is significantly different. This correlates well with the degradation of cells performance after proton irradiation and indicates that the loss in PCE at 10^{14} and 10^{15} protons.cm^{-2} is likely due to degradation of the Spiro-OMeTAD HTL. It has been shown that Spiro-OMeTAD is sensitive to temperature and can undergo strong thermal degradation at 100°C[14]. However, this is very unlikely that the temperature raised to such high temperature during the implantation, even for the highest protons fluence. A low power density of 15 mW.cm^{-2} for the proton beam was used, and the samples were clipped down onto a heat sink which should have enough thermal mass to limit the temperature rise. Unfortunately, it was not possible to measure any potential degradation of the SnO_2 ETL after proton irradiation as the techniques used in this work are not sensitive to such a thin and transparent layer (besides SnO_2 nanoparticles don't have measurable PL or Raman signal). Future work will be necessary to determine the role of SnO_2 ETL in the performance loss due to proton irradiation.

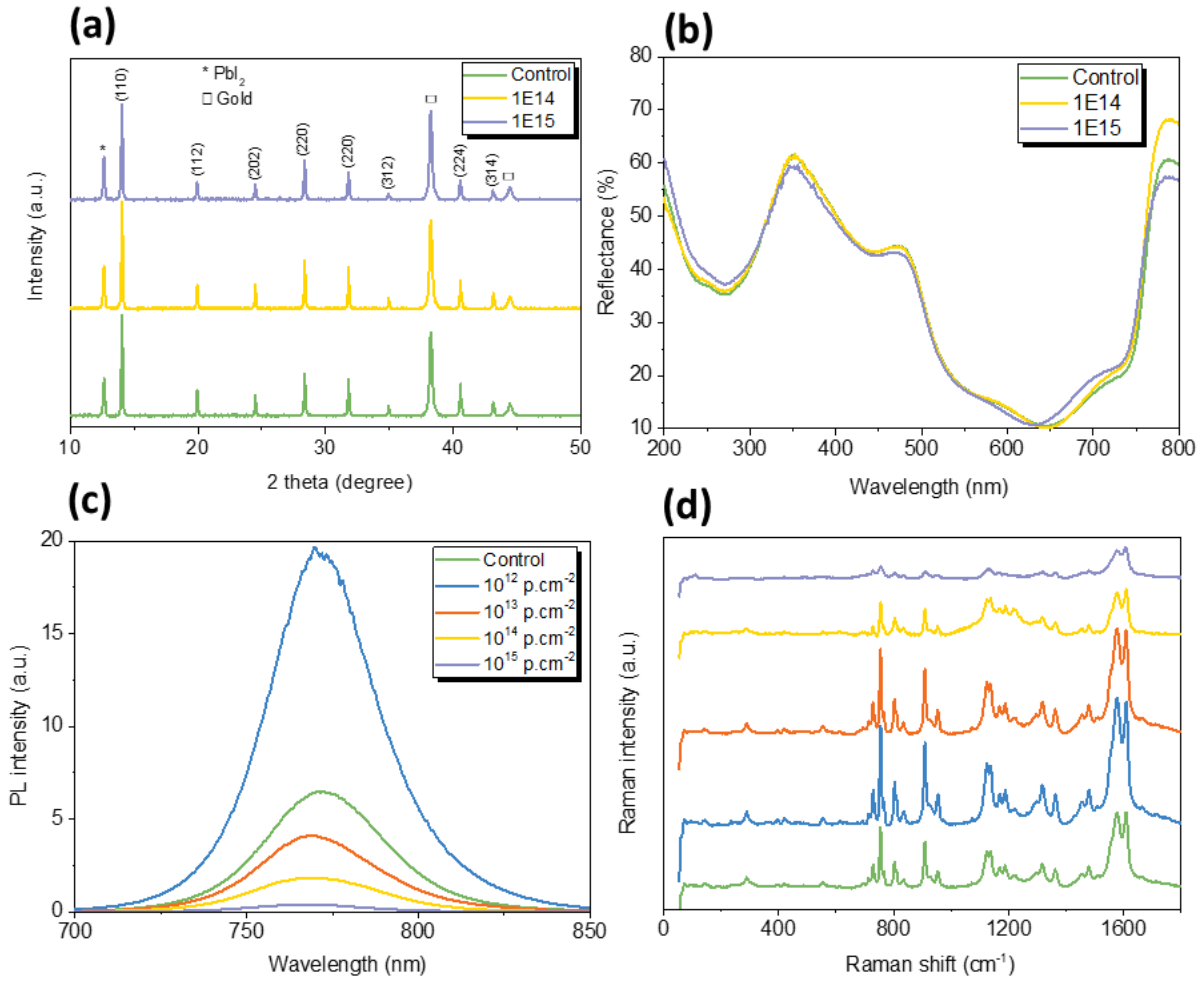

Figure 3. (a) X-ray diffraction spectra of perovskite films deposited on quartz (+ gold electrode) without irradiation and after irradiation with fluences 10^{14} and 10^{15} protons.cm^{-2}. (b) Diffuse reflectance spectra measured with an integrating sphere for perovskite films deposited on quartz (+ gold electrode) without irradiation and after irradiation with fluences 10^{14} and 10^{15} protons.cm^{-2}. (c) Full perovskite solar cells PL intensity as a function of protons fluence. Inset: normalized PL intensity. (d) Raman spectra of perovskite solar cells measured between 0 and 1800 cm^{-1} on top of Spiro-OMeTAD (outside gold electrodes) as a function of protons fluence.

At this stage, we have shown that the Spiro-OMeTAD HTL starts to degrade at 10^{14} protons.cm^{-2}. The crystalline structure and optical properties of the perovskite film remain unchanged up to 10^{14} protons.cm^{-2}, but signs of minor degradation are observed at 10^{15} protons.cm^{-2} from diffuse reflectance measurements. However, these measurements cannot account for local defects created in the perovskite by proton irradiation, such as trap states caused by atomic displacement. In order to study the impact of proton irradiation on recombination within the devices, transient

photovoltage (TPV) measurements were performed. For devices with one dominant recombination mechanism, the perturbed V_{oc} decays back to the steady state with a single exponential time constant[33][34]. This behavior was observed for fluences up to 10^{13} protons.cm^{-2}, indicating that bulk recombination in the perovskite layer is dominating for low proton doses, as shown in Figure 4(a). At 10^{14} protons.cm^{-2}, the TPV decays show clear double exponential behavior at light intensities below 0.25 sun. At higher intensities it is not possible to resolve the additional faster process. Indeed, it is often observed in perovskite cells that bulk recombination is dominant at the highest light intensities, and that underlying mechanisms are only apparent when studied over a range of conditions[34][35][36][37]. This double exponential behavior has been linked to the presence of interfacial recombination, either at the ETL or HTL contacts[38][39][40]. From the observations of Spiro-OMeTAD degradation in the Raman studies, the faster time constant can therefore be attributed to recombination at the perovskite/Spiro interface for this device. It was not possible to study the 10^{15} protons.cm^{-2} device using the standard TPV technique as a stable V_{oc} could not be obtained for this highly degraded device. However, evidence of fast interfacial recombination was observed in the form of a negative transient deflection in response to the laser pulse, as studied in other work (see Figure S6 in SI)[41][42][43].

The charge density in the devices was calculated using the differential capacitance method[44]. Bombardment with 10^{12} and 10^{13} protons.cm^{-2} resulted in a significant increase in charge density as a result of trap formation, as shown in Figure 4(b). A corresponding increase in carrier lifetime suggests that charges spend time in these shallow traps before being released (deeper traps would likely act as recombination centres and cause a decrease in carrier lifetime). Lang et al. have also observed this apparent decrease in the rate of recombination as a result of proton bombardment induced defect formation[11]. This was explained by an efficient trapping/detrapping of minority charge carriers in radiation-induced trap states without major impact on device performance. At 10^{14} protons.cm^{-2}, the additional fast interfacial recombination significantly reduced the carrier lifetime. However, the slower time constant obtained from the double exponential fitting is in the same range as the lifetimes calculated for the lower fluences, suggesting that the bulk recombination lifetime is not significantly reduced at this high fluence. This is consistent with the main source of the performance loss at 10^{14} protons.cm^{-2} being degradation of the Spiro-OMeTAD interface, while trap states formed in the perovskite layer do not affect the performance significantly.

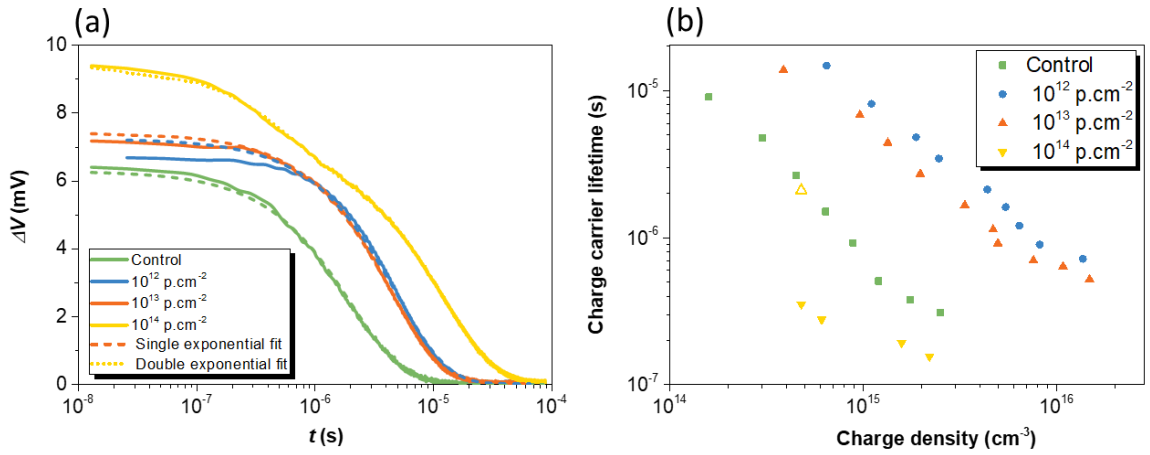

Figure 4: (a) TPV decays for each sample at 0.1 sun equivalent light intensity. Single exponential fitting is suitable for devices up to 10^{13} protons.cm^{-2}. The additional process observed at short times (<1 µs) for the 10^{14} protons.cm^{-2} device results in double exponential fitting being required at that fluence. (b) Charge carrier lifetime versus charge density as a function of proton fluence. Open triangle represents the slower time constant obtained from the double exponential fitting at 10^{14} p.cm^{-2} (device V_{oc} was unstable below this intensity therefore charge density calculation was not possible).

CONCLUSIONS

In summary, the radiation hardness of perovskite solar cells (standard planar architecture) fabricated on AZO/quartz substrates to 150 keV protons has been investigated. Record power conversion efficiency up to 15% has been obtained using low cost, non-toxic, room temperature deposited AZO transparent conductive oxide, which is almost a 3% absolute increase in PCE as compared to previous works. Although a high fraction of the 150 keV protons are stopped in the AZO layer, the optical properties of AZO/quartz substrates remain unchanged, even after irradiation up to 10^{15} protons.cm^{-2}. Perovskite solar cells fabricated on these substrates using a triple cation perovskite active layer and Spiro-OMeTAD HTL show high tolerance to protons radiations up to a fluence of 10^{13} protons.cm^{-2}. In comparison, Si and GaAs solar cells are known to be destroyed or highly deteriorated at this level of radiations. Significant deterioration of the cells is observed at 10^{14} and 10^{15} protons.cm^{-2}, which is ascribed to degradation of the Spiro-OMeTAD HTL during proton irradiation, as shown by degenerated Spiro-OMeTAD Raman spectra, additional interfacial recombination process and hindering of charges extraction properties. Although the structural and optical properties of perovskite remain intact up to high

fluence levels, TPV measurements indicate an increase in minority carrier density and lifetime from 10^{12} protons.cm^{-2}, which is explained by formation of radiation-induced shallow trap states in the perovskite bulk. It is thought that these trap states release charge carriers efficiently and do not affect the performance of the cells for low fluence levels. Therefore, it is demonstrated here that AZO TCO can be promising for perovskite solar cells to be used in space, with both decent PCE and good stability against proton irradiation. Furthermore, this study provides deeper scientific understanding on the interfacial degradation due to proton irradiation, which can be useful for the development of future high PCE perovskite solar cells with ultra-high stability against proton irradiation.

METHODS AND EXPERIMENTAL SECTION

Cell preparation and testing

Quartz glass substrates (UV grade fused silica glass, JGS2, Kintec, Hong Kong) were cleaned by ultrasonication in Hellmanex (2%, deionized water) for 5 minutes, then further sonicated with deionized water for 15 minutes, Acetone for 10 min and then 2-propanol for 5 before being dried via a N_2 gun. AZO (~700 nm) served as a transparent bottom contact was radio-frequency (RF) sputtered using a Moorfield Nanolab 60 sputtering system with power density of 2.46 W.cm^{-2}. The sheet resistance of deposited AZO is 23-25 Ω/□. Before the ETL was deposited, the substrates were treated in oxygen plasma for 5 min. A planar layer of SnO_2 at a thickness of ~25 nm was subsequently deposited via spin coating at a spin speed of 3000 rpm and an acceleration 3000 rpm for 30 s. The SnO_2 precursor solution was fabricated from commercial tin oxide nanoparticles (15% colloidal dispersion in H_2O, Alfa Aesar) diluted in deionized water (1:6.5, volume ratio). This was followed by sintering the substrates at 150°C for 30 min in a fume hood. The triple cation perovskite films were deposited in a N_2 atmosphere using single-step deposition method from the precursor solution containing FAI (172 mg) (Dyesol), PbI_2 (507 mg) (TCI), MABr (22 mg) (Dyesol) and $PbBr_2$ (73 mg) (TCI) in anhydrous N,N-Dimethylformamide (99.8%, Sigma-Aldrich)/dimethylsulphoxide (99.7%, Sigma-Aldrich) (8:2 (v:v)). Thereafter, 53 µL of CsI (99.999% trace metal, Sigma-Aldrich), (390 mg, 1 ml DMSO) was added to the precursor solution. The precursor solution was spin-coated onto the planar SnO_2 films in a two-step program at 1000 and 6000 rpm. for 10 and 20 s, respectively. During the second step, 300 µl of chlorobenzene (99.9%) was dropped on the spinning substrate 5 s prior to the end of the program. This was followed by annealing the films at 100°C for 1 hour. To complete the fabrication of devices, 2,2',7,7'-tetrakis(*N*,*N*-di-*p*-methoxyphenylamine)-9,9-spirobifluorene (Spiro-OMeTAD, 90 mg in chlorobenzene) as a hole-transporting material (HTM) was deposited by spin coating 100 µL of the prepared solution at 4000 rpm for 20 s. The Spiro-OMeTAD (Sigma-Aldrich) was doped with Bis(trifluoromethane)sulfonimide lithium salt (99.95%, Sigma-Aldrich) dissolved in acetonitrile (520 mg/ml), Tris(2-(1H-pyrazol-1-yl)-4-tert-butylpyridine)-cobalt(III) Tris(bis(trifluoromethylsulfonyl)imide) (FK 209, from Dyenamo) and 4-tert-Butylpyridine (96%, Sigma-Aldrich) with concentrations of 34 µL, 10 µL and 19 µL respectively. Finally, device fabrication was completed by thermally evaporating gold wire (99.9% 1mm, Kurt J.Lesker) to form a ~70 nm gold layer as a back contact.

Protons bombardment

The proton beam irradiation was carried out at the Surrey Ion Beam Centre in UK. The reference samples have travelled together with the irradiated samples. All the samples were packed in N_2 atmosphere in the dark during traveling. The reference samples (not irradiated) were exposed to air when the other samples were also exposed to air just before the proton irradiation and during the travel back to Swansea. Sample loading was carried out in a class 100 clean room. The perovskite cells were mounted directly onto 4 in. support plates which were inserted into a carousel wheel in the sample chamber. Silver paste was applied to allow charges to be conducted to the back of the

samples and in the holder plate to avoid charges accumulation. Samples were loaded in a 7°/0° tilt/twist orientation to the incident beam and implanted under vacuum ($2.3 \pm 0.2 \times 10^{-6}$ mbar). The samples were placed to receive direct impact of the protons, with the back contact (gold electrode) facing the proton source. Indeed, the quartz substrate is thick enough to shield the cells from the proton irradiation, so that it would be impossible to measure the effect of protons irradiation on the perovskite layer if the quartz was facing the proton source. A Danfysik 1090 low energy high current implanter was used to implant 150 keV protons into the samples (from the Silver side). The fluence rate was controlled to 3×10^{10}/cm^2.s for fluence 10^{12} protons.cm^{-2} and 3×10^{11}/cm^2.s for fluences 10^{13} to 10^{15} protons.cm^{-2}.

Devices and thin films characterization

UV-Vis Characterization

UV-VIS Transmittance experiments were undertaking on full device structure using a UV/VIS/NIR spectrometer (Lambda 750, PerkinElmer) with an integrating sphere in range 180 to 1000 nm with 1 nm steps. For diffuse reflectance measurements, samples with structure quartz/perovskite/gold where placed on the output port of an integrating sphere with the quartz substrate facing the light beam.

X-Ray diffraction

X-ray diffraction measurements were carried out using a Bruker D8 Discover instrument with a CuKα beam (wavelength is 0.15418 nm) at 40 kV and 40 mA, scan parameters of 1.3 s/step at 0.02° of 2θ step size. All measurements were carried out on samples with structure quartz/perovskite/gold, so that the perovskite crystalline structure was measured through the gold layer.

Raman and PL Characterization

The Raman and PL measurements were performed with a Renishaw inVia Raman system (Renishaw plc., Wotton-Under-Edge, UK) in backscattering configuration. A 532 nm laser and 50x objective were used (NA: 0.50, spot size ≈ 1 μm). For the Raman measurements, a laser power of 150 μW and acquisition time of 10 s were used to measure 25 different points, which were averaged in a single spectrum. For the PL measurements, a laser power of 300 nW and an acquisition time of 2 s were used to measure 121 different points, which were also averaged. Raman spectra of Spiro OMeTAD were measured on the gold side (outside gold electrodes), whereas PL spectra of perovskite film were taken from the glass side.

EQE Measurements

External quantum efficiency (EQE) measurements were made using a monochromatic light source in AC mode with chopping frequency of 70 Hz (QEX10 PV Measurements). The system was calibrated using a NIST-certified calibration cell (PV Measurements) and data points were taken by sweeping the wavelength from 300 to 900 nm and recording a value every 10 nm.

J-V Characterization

The current-voltage (J-V) characteristics of the perovskite devices were recorded with a digital source meter (Keithley model 2400, USA) and 450 W xenon lamp (Sol3A Class AAA Solar Simulator, Oriel, USA). The light source was equipped with an Air Mass filter (Newport) to correct the output of the xenon lamp to better match the AM1.5G solar spectrum. Both forward and reverse bias scans were taken from 1.2 to -0.1 V with a sweep interval of 0.015 V, resulting in 81 data points respectively. The current limit was set to 100 mA.The Air Mass 0 J-V characteristics follow the same experiment set-up and measurement parameters as AM1.5G. However, the AM1.5G filter was replaced with an AM0 filter. Alongside this replacement, the lamp was calibrated by integrating the measured EQE J_{sc} and matching the pixel J_{sc} under the AM0 spectrum with this value.

Transient Photovoltage measurements

TPV measurements were performed using a commercially available transient measurement system (Automatic Research GmbH). This system uses a 635 nm red laser diode driven by a waveform generator (Keysight 33500B) to give a 500 ns pulse length. Background illumination was provided by a white LED with its intensity calibrated to generate the same device photocurrent as measured using the solar simulator - this intensity is referred to as '1 Sun equivalent'. An intensity range was then calibrated using a silicon photodiode. Transient responses were captured by a digital storage oscilloscope (Keysight DSOX2024A), the number of sample averages being adjusted to optimise signal noise and measurement time. The device under test was held at open-circuit by a custom-built voltage follower (1.5 TΩ input impedance). TPC measurements were performed using a current amplifier (Femto DHPCA-100).

AUTHOR INFORMATION

Corresponding Author

*E-mails: jeremy.barbe@swansea.ac.uk, w.c.tsoi@swansea.ac.uk.

Author Contributions

The manuscript was written through contributions of all authors. All authors have given approval to the final version of the manuscript.

CONFLICTS OF INTEREST

There are no conflicts to declare.

ACKNOWLEDGEMENTS

The authors would like to thank Airbus Endeavr Wales for their financial support. The authors would also like acknowledge to the Ser Cymru funding from the Welsh Assembly Government (Ser Solar), the EPSRC fund (Grant No. EP/M025020/1), and the Welsh European Funding Office (SPARC II). The authors would also like to thank the EPSRC through the SPECIFIC Innovation and Knowledge centre Phase 2 (EP/N020863/1). The IMPACT operation has been part-funded by the European Regional Development Fund through the Welsh Government and Swansea University.

REFERENCES

[1] M. A. Green, A. Ho-Baillie, *ACS Energy Lett.* **2017**, *2*, 822.

[2] F. De Rossi, J. A. Baker, D. Beynon, K. E. A. Hooper, S. M. P. Meroni, D. Williams, Z. Wei, A. Yasin, C. Charbonneau, E. H. Jewell, T. M. Watson, *Adv. Mater. Technol.* **2018**,

1800156, 1.

[3] C. Tao, S. Neutzner, L. Colella, S. Marras, A. R. Srimath Kandada, M. Gandini, M. De Bastiani, G. Pace, L. Manna, M. Caironi, C. Bertarelli, A. Petrozza, *Energy Environ. Sci.* **2015**, *8*, 2365.

[4] J. Feng, X. Zhu, Z. Yang, X. Zhang, J. Niu, Z. Wang, S. Zuo, S. Priya, S. (Frank) Liu, D. Yang, *Adv. Mater.* **2018**, *30*, 1.

[5] Nasa Website.

[6] M. Kaltenbrunner, G. Adam, E. D. Głowacki, M. Drack, R. Schwödiauer, L. Leonat, D. H. Apaydin, H. Groiss, M. C. Scharber, M. S. White, N. S. Sariciftci, S. Bauer, *Nat. Mater.* **2015**, *14*, 1032.

[7] AZUR SPACE website.

[8] D. A. Lamb, S. J. C. Irvine, A. J. Clayton, G. Kartopu, V. Barrioz, S. D. Hodgson, M. A. Baker, R. Grilli, J. Hall, C. I. Underwood, R. Kimber, *IEEE J. Photovoltaics* **2016**, *6*, 557.

[9] T. Ohshima, S. I. Sato, T. Nakamura, M. Imaizumi, T. Sugaya, K. Matsubara, S. Niki, A. Takeda, Y. Okano, *Conf. Rec. IEEE Photovolt. Spec. Conf.* **2013**, 2779.

[10] R. M. Burgess, W. S. Chen, W. E. Devaney, D. H. Doyle, N. P. Kim, B. J. Stanbery, Electron and Proton Radiation Effects on GaAs and CuInSe2 Thin Film Solar Cell.

[11] F. Lang, M. Jošt, J. Bundesmann, A. Denker, S. Albrecht, G. Landi, H. C. Neitzert, J. Rappich, N. H. Nickel, *Energy Environ. Sci.* **2019**, 0.

[12] K. Yang, K. Huang, X. Li, S. Zheng, P. Hou, J. Wang, H. Guo, H. Song, B. Li, H. Li, B. Liu, X. Zhong, J. Yang, *Org. Electron. physics, Mater. Appl.* **2019**, *71*, 79.

[13] J.-S. Huang, M. D. Kelzenberg, P. Espinet-Gonzalez, C. Mann, D. Walker, A. Naqavi, N. Vaidya, E. Warmann, H. A. Atwater, **2018**, 1248.

[14] Y. Miyazawa, M. Ikegami, H.-W. Chen, T. Ohshima, M. Imaizumi, K. Hirose, T. Miyasaka, *iScience* **2018**, *2*, 148.

[15] Y. Miyazawa, M. Ikegami, T. Miyasaka, T. Ohshima, M. Imaizumi, K. Hirose, *2015 IEEE 42nd Photovolt. Spec. Conf.* **2015**, 1.

[16] V. V. Brus, F. Lang, J. Bundesmann, S. Seidel, A. Denker, B. Rech, G. Landi, H. C. Neitzert, J. Rappich, N. H. Nickel, *Adv. Electron. Mater.* **2017**, *3*.

[17] F. Lang, N. H. Nickel, J. Bundesmann, S. Seidel, A. Denker, S. Albrecht, V. V. Brus, J. Rappich, B. Rech, G. Landi, H. C. Neitzert, *Adv. Mater.* **2016**, *28*, 8726.

[18] K. Ravichandran, N. Jabena Begum, S. Snega, B. Sakthivel, *Mater. Manuf. Process.* **2016**, *31*, 1411.

[19] H. Lee, E. Lee, T. Noh, M.-S. Jeon, Y. Jeong, *Korean J. Met. Mater.* **2016**, *51*, 145.

[20] R. Pern, F.J., To, B., DeHart, C., Li, X., Glick, S. H., and Noufi, In *SPIE PV Reliability Symposium, 10-14 August 2008, San Diego, California*; 2008.

[21] A. Farooq, I. M. Hossain, S. Moghadamzadeh, J. A. Schwenzer, T. Abzieher, B. S. Richards, E. Klampaftis, U. W. Paetzold, *ACS Appl. Mater. Interfaces* **2018**, *10*, acsami.8b03024.

[22] B. Dou, E. M. Miller, J. A. Christians, E. M. Sanehira, T. R. Klein, F. S. Barnes, S. E. Shaheen, S. M. Garner, S. Ghosh, A. Mallick, D. Basak, M. F. A. M. Van Hest, *J. Phys. Chem. Lett.* **2017**, *8*, 4960.

[23] X. Zhao, H. Shen, Y. Zhang, X. Li, X. Zhao, M. Tai, J. Li, J. Li, X. Li, H. Lin, *ACS Appl. Mater. Interfaces* **2016**, *8*, 7826.

[24] V. La Ferrara, A. De Maria, G. Rametta, M. Della Noce, L. V. Mercaldo, C. Borriello, A. Bruno, P. Delli Veneri, *Mater. Res. Express* **2017**, *4*, 085025.

[25] T.-V. Dang, S. V. N. Pammi, J. Choi, S.-G. Yoon, *Sol. Energy Mater. Sol. Cells* **2017**, *163*, 58.

[26] Z. Hu, S. He, D. Yang, *Mater. Struct.* 150001.

[27] A. K. Jena, Y. Numata, M. Ikegami, T. Miyasaka, *J. Mater. Chem. A* **2018**, *6*, 2219.

[28] Y. Tian, M. Peter, E. Unger, M. Abdellah, K. Zheng, T. Pullerits, A. Yartsev, V. Sundström, I. G. Scheblykin, *Phys. Chem. Chem. Phys.* **2015**, *17*, 24978.

[29] D. W. DeQuilettes, W. Zhang, V. M. Burlakov, D. J. Graham, T. Leijtens, A. Osherov, V. Bulović, H. J. Snaith, D. S. Ginger, S. D. Stranks, *Nat. Commun.* **2016**, *7*.

[30] G. E. Eperon, D. Moerman, D. S. Ginger, *ACS Nano* **2016**, *10*, 10258.

[31] H. Lakhiani, T. Dunlop, F. De Rossi, S. Dimitrov, R. Kerremans, C. Charbonneau, T. Watson, J. Barbé, W. C. Tsoi, *Adv. Funct. Mater.* **2019**, *1900885*, 1900885.

[32] K. E. A. Hooper, H. K. H. Lee, M. J. Newman, S. Meroni, J. Baker, T. M. Watson, W. C. Tsoi, *Phys. Chem. Chem. Phys.* **2017**, *19*, 5246.

[33] L. Contreras-Bernal, M. Salado, A. Todinova, L. Calio, S. Ahmad, J. Idígoras, J. A. Anta, *J. Phys. Chem. C* **2017**, *121*, 9705.

[34] J.-P. Correa-Baena, S.-H. Turren-Cruz, W. Tress, A. Hagfeldt, C. Aranda, L. Shooshtari, J. Bisquert, A. Guerrero, *ACS Energy Lett.* **2017**, *2*, 681.

[35] A. Pockett, G. E. Eperon, T. Peltola, H. J. Snaith, A. Walker, L. M. Peter, P. J. Cameron, *J. Phys. Chem. C* **2015**, *119*, 3456.

[36] B. Smith, J. Troughton, A. Lewis, J. McGettrick, A. Pockett, M. Carnie, C. Charbonneau, C. Pleydell- Pearce, J. Searle, P. Warren, S. Varma, T. Watson, *Adv. Mater. Interfaces* **2019**, *6*, 1801773.

[37] L. Gouda, R. Gottesman, A. Ginsburg, D. A. Keller, E. Haltzi, J. Hu, S. Tirosh, A. Y. Anderson, A. Zaban, P. P. Boix, *J. Phys. Chem. Lett.* **2015**, *6*, 4640.

[38] M. J. Carnie, C. Charbonneau, M. L. Davies, B. O. Regan, D. A. Worsley, T. M. Watson, *J. Mater. Chem. A* **2014**, *2*, 17077.

[39] N. F. Montcada, J. M. Marín-Beloqui, W. Cambarau, J. Jiménez-López, L. Cabau, K. T. Cho, M. K. Nazeeruddin, E. Palomares, *ACS Energy Lett.* **2017**, *2*, 182.

[40] B. C. O'Regan, P. R. F. Barnes, X. Li, C. Law, E. Palomares, J. M. Marin-Beloqui, *J. Am. Chem. Soc.* **2015**, *137*, 5087.

[41] A. Pockett, M. J. Carnie, *ACS Energy Lett.* **2017**, 1683.

[42] P. Calado, A. M. Telford, D. Bryant, X. Li, J. Nelson, B. C. O'Regan, P. R. F. Barnes, *Nat. Commun.* **2016**, *7*, 13831.

[43] T. W. and M. C. A. Pockett, D. Raptis, S. M. P. Meroni, J. Baker, *J. Phys. Chem. C* **2019**.

[44] C. G. Shuttle, B. O'Regan, A. M. Ballantyne, J. Nelson, D. D. C. Bradley, J. de Mello, J. R. Durrant, *Appl. Phys. Lett.* **2008**, *92*, 093311.

1

2

SUPPORTING INFORMATION

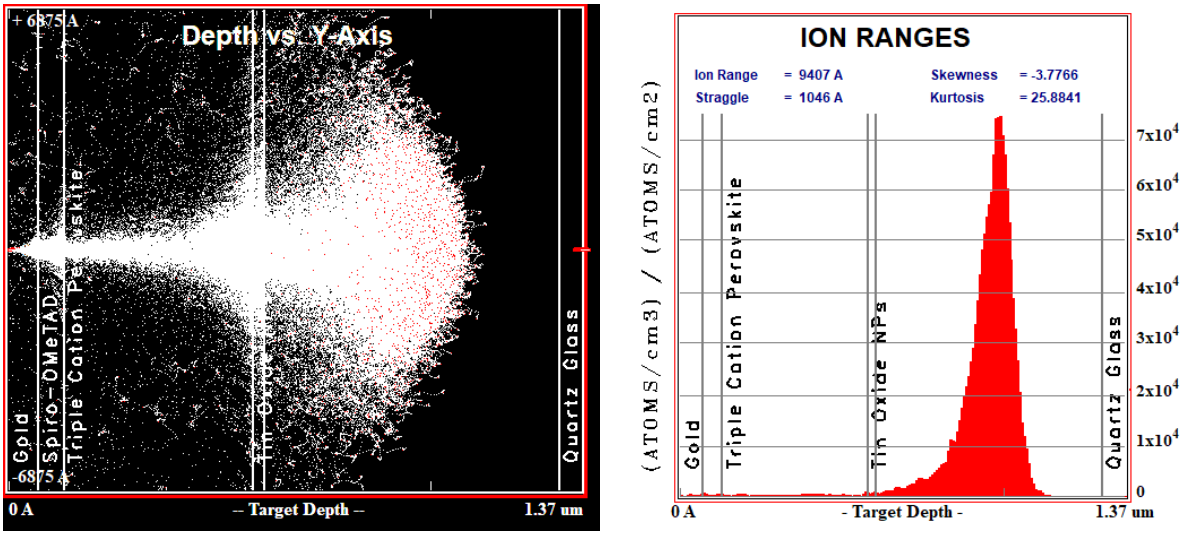

Figure S1. SRIMS Simulation of the perovskite cells undergoing particle bombardment at 150 keV from the gold side. Schematic diagram with particle stopping points (left) and Ion Ranges histogram (right), shows that the AZO acts as a barrier and stops nearly all protons with this energy.

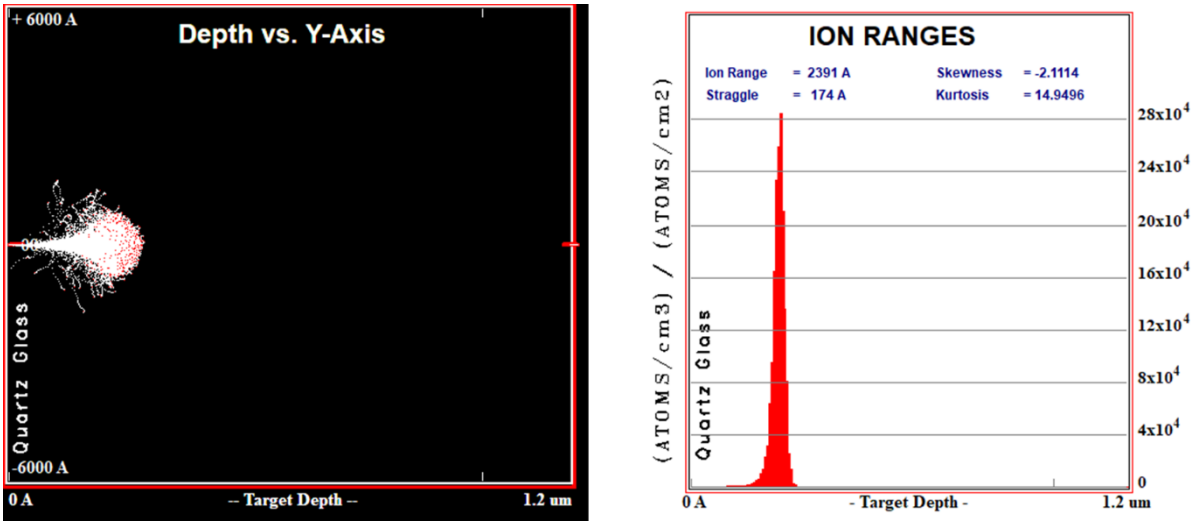

Figure S2. SRIMS Simulation of a quartz substrate undergoing particle bombardment at 150 keV. Schematic diagram with particle stopping points (left) and Ion Ranges histogram (right), show that all protons with this energy are stopped in the first 230 nm of the 1 mm quartz substrate.

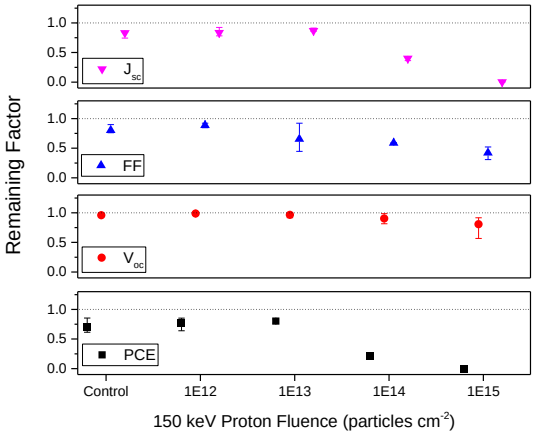

Figure S3. Changes of photovoltaic characteristics (J_{sc}, FF, V_{oc}, and PCE) of perovskite solar cells under AM0 illumination as a function of protons fluence. Averaged values measured for a total of 6 different cells for each fluence

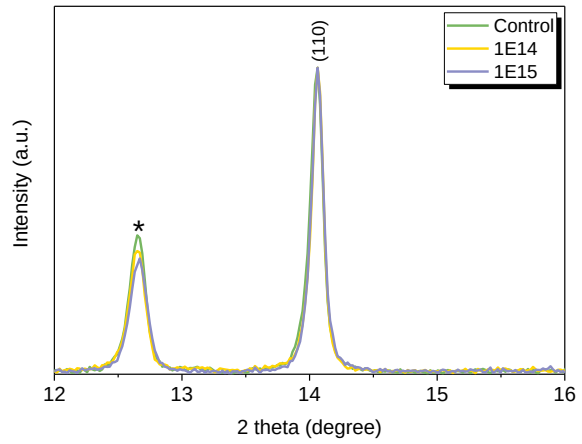

Figure S4. Normalized XRD spectra of perovskite thin films on quartz for control sample and samples irradiated with 10^{14} and 10^{15} protons.cm^{-2}

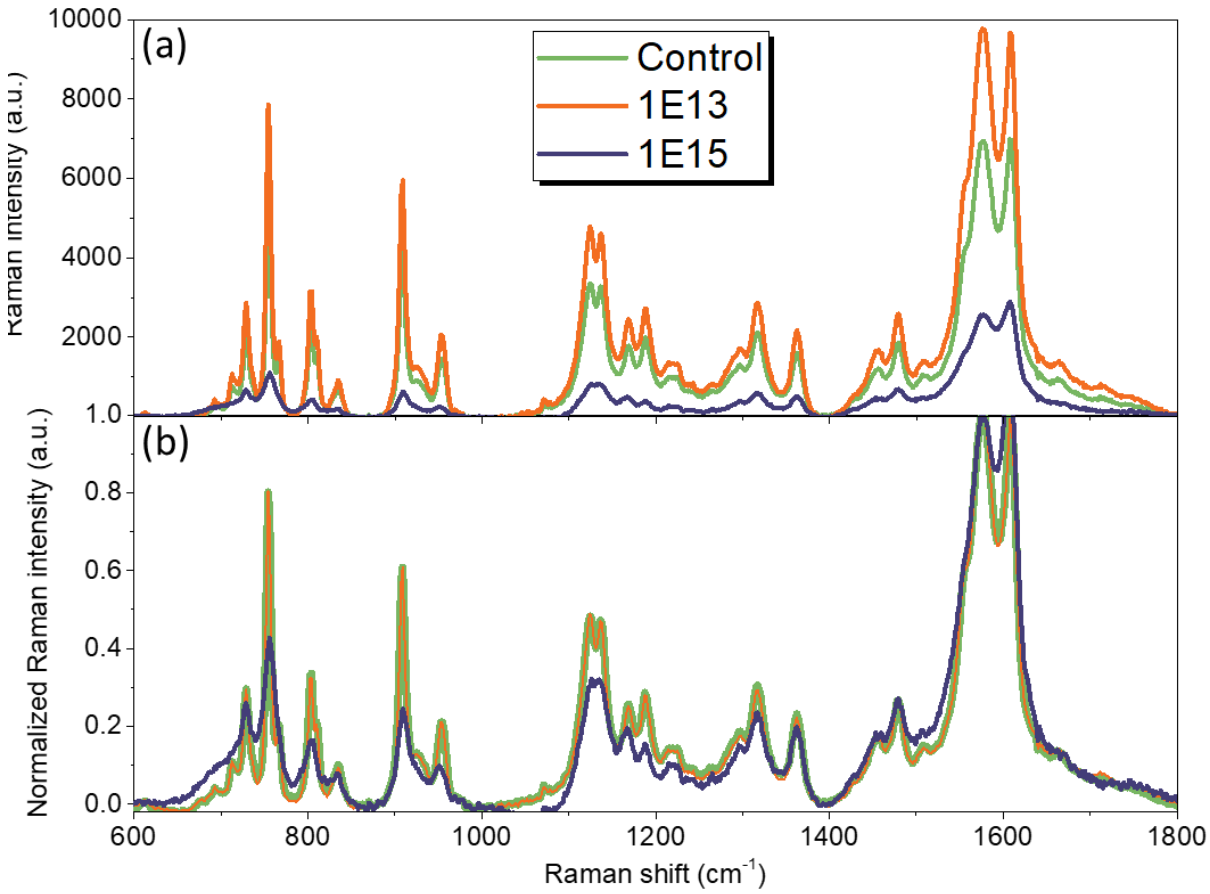

Figure S5. (a) Raman spectra of Spiro OMeTAD for the control sample and sample irradiated with 10^{13} and 10^{15} protons.cm^{-2}. (b) Same spectra after normalization (divided by intensity at 1575 cm^{-1}).

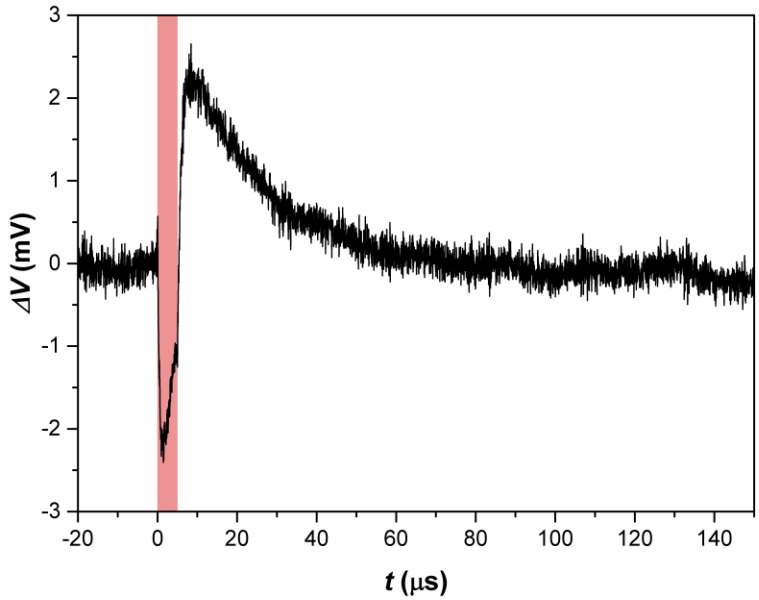

Figure S6. TPV response for device bombarded with 10^{15} protons.cm^{-2} measured at 1 Sun equivalent intensity. Laser pulse (red shaded region) induces a rapid negative deflection (decrease in V_{oc}) in the TPV response indicative of fast interfacial recombination.